

Harnessing Chiral Spin States in Molecular Nanomagnets for Quantum Technologies

Aman Ullah, Ziqi Hu, Juan Aragó, and Alejandro Gaita-Ariño

Instituto de Ciencia Molecular (ICMol), Universitat de València, Paterna, Spain

We present a theoretical framework to investigate spin chirality in molecular quantum systems. Focusing on a minimal three-spin-center model with antiferromagnetic exchange and symmetry breaking—driven by an electric-field-induced Dzyaloshinskii-Moriya interaction and applied magnetic fields—give rise to chiral ground states characterized by nonzero scalar spin chirality, $\chi = \mathbf{S}_1 \cdot (\mathbf{S}_r \times \mathbf{S}_2)$. The emergent chiral qubits naturally suppress always-on interactions that can not be switched off in weakly coupled qubits, as demonstrated through Liouville–von Neumann dynamics, which reveal phase difference in superposition states that form chiral qubits. To validate this framework, we examine realistic lanthanide complexes with radical-bridged magnetic centers, where spin-orbit coupling and asymmetric exchange facilitate chirality. Our findings establish spin chirality engineering as a promising strategy for mitigating always-on interaction in entangling two chiral qubits in molecular quantum technologies.

Spin chirality offers a promising pathway for quantum initialization by mitigating always-on interactions [1, 2]. It can emerge intrinsically from a molecular structure [3] or be engineered through spin-chiral state creation [4]. In the latter case, chiral states can arise from photoexcited triplets, with quantum initialization achieved via microwave-driven population transfer [5–8]. In the former case, chirality has been extensively studied in spin-frustrated triangles, where the spin spectrum provides a rich platform for chiral phenomena [9–11]. Experimental realization of spin chirality typically requires application of

external fields, both electric and magnetic [12]. However, this approach is hindered by the intrinsically weak spin-electric coupling in most systems.

Lanthanide-based molecular nanomagnets present a compelling solution to this challenge, which have been shown to exhibit strong spin-electric coupling with their 4f electronic structures [13]. These properties make lanthanide nanomagnets particularly advantageous for quantum operations. Previous Lanthanide based molecular qubit candidates have been proven to show robust quantum coherence. Towards quantum entanglement among different qubits, however, they suffer from the problem of always-on inter-qubit communication in the form of weak magnetic coupling, which cannot be switched off during the qubit operations [14–16]. In this context, chiral qubits offer an ideal platform to effectively quench the always-on interaction [17, 18]. Among the lanthanide-based qubit candidates, dinuclear lanthanide complexes bridged by a radical ligand (Ln^{3+} –radical– Ln^{3+}), stand out due to their exceptional magnetic and electronic properties [19–21]. The interplay between the spin-orbit coupling of lanthanide ions and the delocalized spin density of the radical creates a unique environment for enhanced coupling to external electric potentials.

In a Ln^{3+} –radical– Ln^{3+} molecular system, the emergence of spin chirality and Dzyaloshinskii–Moriya (DM) interactions requires the breaking of specific symmetries. When inversion symmetry is preserved (e.g., at equilibrium), the radical-mediated superexchange interactions are symmetric, suppressing both spin chirality and antisymmetric exchange. However, an external electric field breaks inversion symmetry by polarizing the electronic environment, creating asymmetric hopping pathways between the Ln^{3+} ions via the radical bridge. This asymmetry,

Aman Ullah: aman.ullah@uv.es

Alejandro Gaita-Ariño: alejandro.gaita@uv.es

combined with spin-orbit coupling (either from the radical or ligand orbitals), generates a finite DM vector, which introduces non-collinear spin textures and chirality. Also, breaking time-reversal symmetry via magnetic field is necessary to remove the degeneracy between chiral states (e.g., clockwise vs. counterclockwise spin rotation), thereby stabilizing a specific chirality. Consequently, dual-field control is vital: the electric field initiates chirality by disrupting spatial symmetry, while the magnetic field determines the chiral ground state by breaking time-reversal symmetry.

In this work, we first develop and validate a theoretical framework for spin chirality using a minimal three spin-1/2 system, where controlled symmetry breaking—of both time-reversal (via magnetic field) and inversion (via electric-field-induced DM interaction)—enables the emergence of chiral states. We then employ this validated model to demonstrate the existence of robust chiral spin states in a dinuclear lanthanide-based single-molecule magnet [22]. The effective Hamiltonian combines intrinsic terms (spin Hamiltonian and exchange interactions) with extrinsic control terms (Zeeman and Dzyaloshinskii-Moriya interactions). Our calculations of the scalar spin chirality (χ) reveal distinct phase-locked states within the ground-state doublet, while stochastic Liouville simulations confirm that these chiral states maintain persistent phase relationships under dynamics [23], crucially exhibiting the ability to suppress always-on interactions through engineered phase interference.

1 Model

In a system of three spin-1/2 centers, two lanthanide ions (S_1, S_2) are bridged by a radical spin (S_r), with anisotropic anti-ferromagnetic (AFM) exchange ($J_x = J_y \neq J_z$) and g -tensor anisotropy ($g_x = g_y \neq g_z$), both favoring spin alignment along the z -axis. While this anisotropy typically stabilizes a collinear ground state, spin chirality—quantified by the scalar $\chi = \mathbf{S}_1 \cdot (\mathbf{S}_r \times \mathbf{S}_2)$ —vanishes unless inversion symmetry is broken. To induce chirality, we apply an in-plane electric field, which acts as a polar vector to break inversion symmetry. This generates a Dzyaloshinskii-Moriya (DM) interaction in the form of $\hat{H}_{DM} = \sum_{\langle i,j \rangle} \mathbf{D}_{ij}(E) \cdot (\mathbf{S}_i \times \mathbf{S}_j)$. Here,

the DM vector arises from spin-orbit coupling and radical-mediated asymmetric exchange (Fig. 1a). The DM interaction promotes non-collinear spin textures in the x - y plane, competing with the z -axis anisotropy. This competition stabilizes a chiral ground state with non-coplanar spin configurations and finite χ , where the handedness is determined by the relative orientation of the spins.

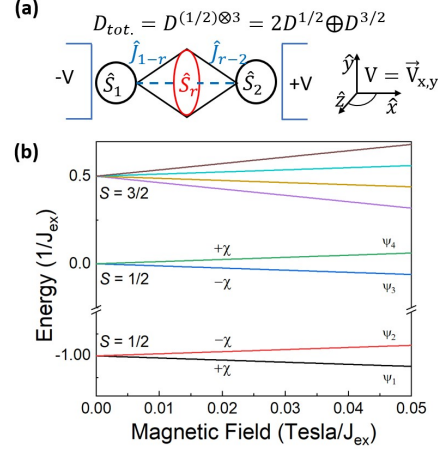


Figure 1: **(a)**—Two spin-1/2 centers (\hat{S}_1 and \hat{S}_2) are linked through a radical bridge (\hat{S}_{rad}) via AFM exchange couplings \hat{J}_{1-r} , \hat{J}_{r-2} , \hat{J}_{21} . The energy spectrum contains two spin doublets ($2D^{1/2}$) and one quartet ($D^{3/2}$). **(b)**—In an AFM exchange, the splitting in two-doublet is proportional to J_{ex} , the quartet is separated by higher in energy doublet by $J_{ex}/2$.

The effective Hamiltonian for dinuclear lanthanide ions (S_1, S_2) coupled via a radical bridge (S_r) is given by:

$$\hat{H}_{eff} = \hat{H}_S + \hat{H}_{ex} + \hat{H}_B + \hat{H}_{DM} \quad (1)$$

\hat{H}_S is zero-field splitting (ZFS) Hamiltonian defined as:

$$\hat{H}_S = \sum_{\alpha=1,2} [D_{\alpha} (\hat{S}_{\alpha z}^2 - S_{\alpha}(S_{\alpha} + 1)/3) + E_{\alpha} (\hat{S}_{\alpha+}^2 + \hat{S}_{\alpha-}^2)/2] \quad (2)$$

where D (axial) and E (rhombic) indicate ZFS parameters for the spin centers, $\alpha = 1, 2$, and $\hat{S}_{\alpha\pm} = \hat{S}_{\alpha x} \pm i\hat{S}_{\alpha y}$ are spin ladder operators. The terms \hat{H}_{ex} and \hat{H}_B represent exchange and Zeeman Hamiltonians respectively, which are defined as;

$$\hat{H}_{ex} = J_{1-r}\hat{S}_1\hat{S}_r + J_{r-2}\hat{S}_r\hat{S}_2 + J_{2-1}\hat{S}_2\hat{S}_1 \quad (3)$$

$$\hat{H}_B = g_1\mu_B B\hat{S}_1 + g_r\mu_B B\hat{S}_r + g_2\mu_B B\hat{S}_2 \quad (4)$$

where $J_{ij} < 0$ accounts for antiferromagnetic exchange between spins; J_{1r} and J_{r2} are the strong radical-lanthanide couplings, which overwhelm the weak lanthanide-lanthanide coupling J_{12} ; $g_{1,r,2}$ are the g -tensors, μ_B is the Bohr magneton, and B is the magnetic field. The DM Hamiltonian (\hat{H}_{DM}) arises because of an external electric potential, which is defined as:

$$\hat{H}_{DM} = \sum_{\langle i,j \rangle} \mathbf{D}_{ij}(E) \cdot (\mathbf{S}_i \times \mathbf{S}_j) \quad (5)$$

where $\langle i,j \rangle$ denotes all unique pairs of spins $((1,r), (r,2), \text{ and } (1,2))$. The DM interaction can be compactly expressed using the Levi-Civita symbol $\epsilon_{\alpha\beta\gamma}$, where $\alpha, \beta, \gamma \in \{x, y, z\}$ to explicitly capture its antisymmetric nature:

$$\hat{H}_{DM} = \sum_{\alpha,\beta,\gamma} \epsilon_{\alpha\beta\gamma} (D_{1r}^\alpha S_1^\beta S_r^\gamma + D_{r2}^\alpha S_r^\beta S_2^\gamma + D_{12}^\alpha S_1^\beta S_2^\gamma) \quad (6)$$

The DM interaction imposes specific phase relationships, resulting in a non-coplanar configuration. The scalar chirality is captured by the expectation value:

$$\langle \chi \rangle = \langle \psi_i | \mathbf{S}_1 \cdot (\mathbf{S}_r \times \mathbf{S}_2) | \psi_i \rangle \quad (7)$$

where $|\psi\rangle$ is the i -th eigenfunction of the effective Hamiltonian. This becomes nonzero due to the antisymmetric contributions of the DM interaction. The sign of $\langle \chi \rangle$ distinguishes between right- and left-handed spin configurations, making the primary carriers of spin chirality in this system.

For our numerical analysis, we work with a dimensionless form of the effective Hamiltonian obtained by scaling all terms by the dominant exchange coupling constant J_{ex} , yielding $\hat{H} = H_{\text{eff}}/J_{ex}$. This normalization reveals two key dimensionless parameters: (1) the Zeeman ratio $\text{Zeeman} = \mu_B g J B / J_{ex}$ and (2) the DM interaction ratio $\text{DR} = D_{ij} / J_{ex}$. Typical experimental values place the DM interaction in the range of $10^{-2} \text{ cm}^{-1} \rightarrow 1 \text{ cm}^{-1}$ [24, 25], and exchange coupling between $10 \text{ cm}^{-1} \rightarrow 10^2 \text{ cm}^{-1}$ [26, 27], for lanthanide-based nanomagnets, resulting in DR values for $\text{DR}(D_{ij}^x, D_{ij}^y) \in [10^{-4}, 10^{-1}]$. The magnetic field dependence of the scaled energy levels is shown in Fig. 1b. Analysis of the two $S = 1/2$ state wavefunctions at $(D_{ij}^x = 0.1, D_{ij}^y = 0.1)$ reveals a distinct chiral character. The calculated

scalar chirality and wavefunction composition for two $S = 1/2$ is provided in table 1.

To map the chiral texture of the ground states, we defined two spin-based vector field operators:

$$\hat{S}_x = \hat{S}_1^x \otimes \hat{S}_r^z \otimes \hat{S}_2^x, \quad \hat{S}_y = \hat{S}_1^y \otimes \hat{S}_r^z \otimes \hat{S}_2^y \quad (8)$$

where \hat{S}_i^α are spin-1/2 operators for site i and $\alpha = x, y, z$. These operators probe the coupled spin correlations between S_1 and S_2 , modulated by the z -polarization of the radical spin \hat{S}_r . For each eigenstate $|\psi_i\rangle$, the vector field components (v_x, v_y) are calculated $v_x = \langle \psi_i | \hat{S}_x | \psi_i \rangle$, $v_y = \langle \psi_i | \hat{S}_y | \psi_i \rangle$. The field's magnitude ($|v| = \sqrt{v_x^2 + v_y^2}$) and phase angle ($\theta = \tan^{-1}(v_y/v_x)$) were evaluated across the DM parameter space $[-D_x, -D_y] \times [-D_x, -D_y]$. The vector field's vorticity (curl) is directly tied to the DM strength (D_x, D_y) . Regions with larger $|D_{ij}|$ exhibit stronger non-coplanar spin alignment, leading to higher field magnitudes $|v|$. The vector fields for the two ground doublets ($|\psi_1\rangle, |\psi_2\rangle$ and $|\psi_3\rangle, |\psi_4\rangle$) are mirror images of each other (Fig. 2). This reflects the opposite chiralities imposed by the DM interaction, where $|\psi_1\rangle, |\psi_2\rangle$ form a left-handed chiral qubit and $|\psi_3\rangle, |\psi_4\rangle$ exhibits right-handed chiral qubit.

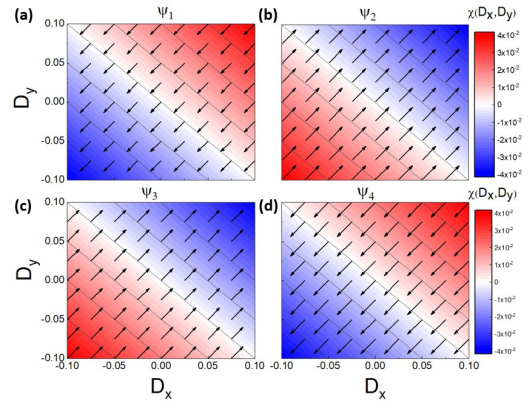


Figure 2: **(a)-(d)**- Variation of scalar chirality (χ) and vector field of $|\psi_1\rangle, |\psi_2\rangle, |\psi_3\rangle$, and $|\psi_4\rangle$ in DM parameter space $[-D_x, -D_y] \times [-D_x, -D_y]$ and $\{B_x, B_y, B_z\} = \{0.01, 0.01, 0.02\}$.

1.1 Quenching Always-On Interactions with Chirality

In a chiral quantum system, we consider two qubits, A and B, initialized in superposition

Table 1: Wave function composition of ground and first excited doublet at ($D_{ij}^x = D_{ij}^y = 0.1$) and $\{B_x, B_y, B_z\} = \{0.01, 0.01, 0.02\}$.

Eigen-state	χ	Energy ($1/J_{ex}$)	Wave-function
ψ_1	+ 0.04	0.0000	15% $ \uparrow_1\downarrow_r\downarrow_2\rangle + 60\% \downarrow_1\uparrow_r\downarrow_2\rangle + 15\% \downarrow_1\downarrow_r\uparrow_2\rangle$
ψ_3	- 0.04	0.0479	15% $ \uparrow_1\uparrow_r\downarrow_2\rangle + 60\% \uparrow_1\downarrow_r\uparrow_2\rangle + 15\% \downarrow_1\uparrow_r\uparrow_2\rangle$
ψ_4	- 0.04	1.0006	5% $ \uparrow_1\uparrow_r\downarrow_2\rangle + 45\% \uparrow_1\downarrow_r\downarrow_2\rangle + 5\% \downarrow_1\uparrow_r\uparrow_2\rangle + 45\% \downarrow_1\downarrow_r\uparrow_2\rangle$
ψ_5	+ 0.04	1.0551	5% $ \uparrow_1\uparrow_r\downarrow_2\rangle + 45\% \uparrow_1\downarrow_r\downarrow_2\rangle + 5\% \downarrow_1\uparrow_r\uparrow_2\rangle + 45\% \downarrow_1\downarrow_r\uparrow_2\rangle$

states with distinct chiral phases, termed chiral doublets. These states are defined as:

$$(\psi_1, \psi_2) = (\chi, -\chi) \rightarrow |\psi_A\rangle = \frac{1}{\sqrt{2}}(|0\rangle - |1\rangle), \quad (9)$$

$$(\psi_3, \psi_4) = (-\chi, \chi) \rightarrow |\psi_B\rangle = \frac{1}{\sqrt{2}}(-|0\rangle + |1\rangle), \quad (10)$$

where χ denotes a scalar chirality parameter. These configurations resemble left- and right-handed states, analogous to chiral systems in condensed matter or particle physics. The initial tensor product of these doublets is: $|\psi_A\rangle \otimes |\psi_B\rangle \frac{1}{2}(-|00\rangle + |01\rangle - |10\rangle + |11\rangle)$. To entangle them, we apply a CNOT gate (A as control, B as target), transforming the basis states: $|00\rangle \rightarrow |00\rangle$, $|01\rangle \rightarrow |01\rangle$, $|10\rangle \rightarrow |11\rangle$, $|11\rangle \rightarrow |10\rangle$. This yields the entangled state:

$$|\psi\rangle = \frac{1}{2}(-|00\rangle + |01\rangle + |10\rangle - |11\rangle). \quad (11)$$

This state embeds the chiral properties of the doublets and is pivotal for mitigating unwanted interactions.

Let us now examine an always-on interaction between the qubits, modeled by the Hamiltonian:

$$\hat{H} = J\hat{\sigma}_z^A \otimes \hat{\sigma}_z^B, \quad (12)$$

where J is the coupling strength and $\hat{\sigma}_z$ is the Pauli-Z operator. Such interactions are persistent and can disrupt quantum control in multi-qubit systems. Our objective is to demonstrate that the chiral entangled state $|\psi\rangle$ quenches this interaction, reducing its expectation value to zero. For $|\psi\rangle = \frac{1}{2}(-|00\rangle + |01\rangle + |10\rangle - |11\rangle)$, we evaluate $\hat{\sigma}_z^A \hat{\sigma}_z^B$:

$$\begin{aligned} \hat{\sigma}_z^A \hat{\sigma}_z^B |00\rangle &= +|00\rangle \quad (\text{eigenvalue } +1), \\ \hat{\sigma}_z^A \hat{\sigma}_z^B |01\rangle &= -|01\rangle \quad (\text{eigenvalue } -1), \\ \hat{\sigma}_z^A \hat{\sigma}_z^B |10\rangle &= -|10\rangle \quad (\text{eigenvalue } -1), \\ \hat{\sigma}_z^A \hat{\sigma}_z^B |11\rangle &= +|11\rangle \quad (\text{eigenvalue } +1). \end{aligned}$$

Applying this operator:

$$\sigma_z^A \sigma_z^B |\psi\rangle = \frac{1}{2}(-|00\rangle - |01\rangle - |10\rangle + |11\rangle). \quad (13)$$

The expectation value is:

$$\langle \psi | \hat{\sigma}_z^A \hat{\sigma}_z^B | \psi \rangle = 0 \quad (14)$$

Thus, $\langle \hat{H} \rangle = J \cdot 0 = 0$. The chiral phases induce destructive interference, neutralizing the effect of the interaction. To realize this state, we construct a quantum circuit starting from $|0\rangle_A |0\rangle_B$. Hadamard gates (H) generate superpositions: $H|0\rangle = \frac{1}{\sqrt{2}}(|0\rangle + |1\rangle)$. For qubit A, a Z -gate adjusts the phase to produce $|\psi_A\rangle$. For qubit B, an $R_z(\pi)$ gate, defined as $R_z(\pi) = \begin{pmatrix} -i & 0 \\ 0 & i \end{pmatrix}$, followed by H , yields $|\psi_B\rangle$ up to a global phase. A CNOT gate then entangles the qubits:

$$\begin{array}{c} |0\rangle_A \text{---} [H] \text{---} [Z] \text{---} \bullet \\ |0\rangle_B \text{---} [H] \text{---} [R_z(\pi)] \text{---} \oplus \end{array} \quad (15)$$

Without chirality, the interaction remains unmitigated, as the state aligns with the Hamiltonian's eigenstates, offering no cancellation. The chiral entangled state leverages phase differences to quench the always-on interaction, a feature absent in the non-chiral case, highlighting the utility of chirality in quantum control.

1.2 Chirality induced time dynamics

The presence of chirality in the spin spectrum as a result of the DM interaction alters the overall dynamics, results in precessional dynamics of the spins driving the spins into a non-coplanar configuration over time such as dephasing times (T_1 and T_2). Radical-bridged lanthanide systems involve lanthanide ions (e.g., Dy(III), Tb(III),

Gd(III)) coupled via organic radicals (e.g., nitroxides, N_2^{3-} , semiquinones), which enhance magnetic exchange and influence relaxation times. T_1 reflects energy transfer between spins and the lattice (phonons), while T_2 measures coherence loss due to spin-spin interactions or local magnetic noise (e.g., hyperfine coupling). In these systems, cryogenic temperatures (≤ 2 K or 2–4 K) often yield T_1 in the microsecond range (e.g., 0.1–1 μs) and T_2 in the nanosecond to microsecond range (e.g., 10–100 ns), depending on the radical and environment [19, 28]. These factors are considered by evaluating the time evolution of the density matrix using the stochastic Liouville equation [23], considering both coherent and incoherent contributions.

$$\frac{\partial \rho(t)}{\partial t} = -\frac{i}{\hbar} [\omega_{ab}, \rho] + \hat{\mathbf{L}}\rho \quad (16)$$

where, $\omega_{\alpha\beta} = (E_\alpha - E_\beta)$, and E_α and E_β are the corresponding eigenvalues, $\hat{\mathbf{L}}$ is the dissipation super operator which contains both transverse and longitudinal relaxation rates.

$$\hat{\mathbf{L}} = -\frac{1}{T_1^{\alpha\alpha\&\beta\beta}} - \frac{1}{T_2^{\alpha\beta\&\beta\alpha}} \quad (17)$$

, where α and β run over the eigenstates of the effective Hamiltonian. The initial states for qubit A and B are prepared, $|\psi_A\rangle = 1/\sqrt{2}(\psi_1 + \psi_2)$, $|\psi_B\rangle = 1/\sqrt{2}(\psi_3 + \psi_4)$, respectively. The corresponding density at time(t)=0 is, $\rho_A(0) = |\psi_A(0)\rangle\langle\psi_A(0)|$ and $\rho_B(0) = |\psi_B(0)\rangle\langle\psi_B(0)|$. We track the evolution of chirality ($\chi(t)$) by:

$$\langle\chi_{(A,B)}(t)|\chi_{(A,B)}(t)\rangle = \text{Tr}(\rho_{(A,B)}(t)\chi) \quad (18)$$

Fig. 3, shows the time evolution of chiral expectation values $\langle\chi_A(t)|\chi_A(t)\rangle$ and $\langle\chi_B(t)|\chi_B(t)\rangle$ for superposition states $|\psi_A\rangle$ and $|\psi_B\rangle$. The phase difference reflects chiral symmetry breaking from the DM interaction, with oscillations indicating coherent dynamics.

2 Case Study

For our case study, we consider the N_2^{3-} radical bridging ligand N_2^{3-} in the centrosymmetric molecule (Fig. 4) [22]. The delocalized unpaired electron on the ligand mediates a strong antiferromagnetic coupling between Gd^{3+} and the unpaired electron (-27 cm^{-1} in $-2JS_1S_2$ formalism).

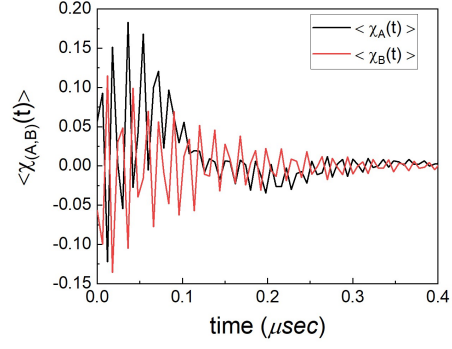


Figure 3: Time-evolution of chiral-expectation value for qubit-A and qubit-B.

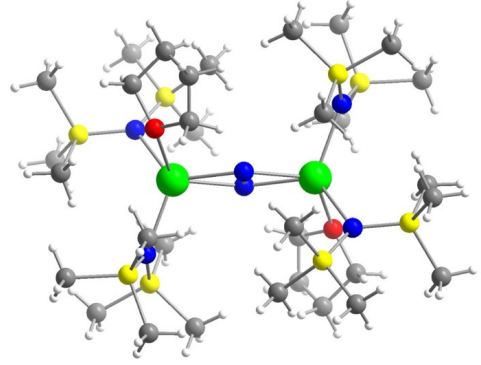


Figure 4: A dinuclear Gd- N_2 -Gd complex: Green, Gd; blue, N; red oxygen; yellow, Si.

This coupling dominates the weak Gd^{3+} - Gd^{3+} interaction ($J = 0.07 \text{ cm}^{-1}$).

The time-independent electronic structures of Gd-Y and Y-Gd fragments were performed using the multiconfigurational Complete Active Self-Consistent Field Spin-Orbit (CASSCF-SO) method implemented in the OpenMOLCAS program package (version 18.09) [29]. Scalar relativistic effects were considered with Douglas-Kroll-Hess transformation using ANO-RCC-VDZP basis set for all atoms. The active space consisted of 7 electrons on the 7 f -orbitals of Gd^{3+} ion. The molecular orbitals were optimized at the CASSCF level in a state average (SA) over an octet ($S = 7/2$), 48 sextet ($S = 5/2$), 120 quartet ($S = 3/2$) and 113 doublets ($S = 1/2$). The wave functions obtained at CASSCF were then mixed by spin-orbit coupling by means of the RASSI approach. The crystal field parameters (D and E provided in table 2) used for the system Hamiltonian were calculated using SINGLE_ANISO module implemented in OpenMOLCAS [30].

Table 2: D and E parameters determined at *ab-initio* level.

	D (cm^{-1})	E (cm^{-1})
Gd-Y	-0.0489	-0.0561
Y-Gd	-0.0489	-0.0562

The spin spectrum, including exchange and Zeeman interactions, was calculated using the D and E parameters listed in Table 2. The total Hilbert space comprises 128 states, accounting for the two Gd^{3+} ions ($S_1 = S_2 = 7/2$) and a central radical spin ($S_r = 1/2$). The ground-state multiplet has an $S = 13/2$ due to the strong antiferromagnetic (AF) exchange between the Gd^{3+} ions and the radical. Excited multiplets with $S = 11/2$, $S = 9/2$, $S = 7/2$, $S = 5/2$, $S = 3/2$, $S = 1/2$, $S = 1/2$, $S = 3/2$, $S = 5/2$, $S = 7/2$, $S = 9/2$, $S = 11/2$, $S = 13/2$ and finally $S = 15/2$. The effective Hamiltonian (Eq. 1) includes the Dzyaloshinskii-Moriya (DM) interaction term $\hat{H}_{DM}(E)$, with $|D(E)| \approx 1 \text{ cm}^{-1}$. For excited multiplets ($S = 1/2, 1/2, 3/2$), the system forms two doublets and a quartet, analogous to three spin-1/2 centers coupled via AF exchange. However, the presence of Gd^{3+} 4*f* electrons—with their large orbital angular momentum (\hat{L}) and strong spin-orbit coupling—enhances the spin-electric response. To simplify the high-dimensional problem, we restricted the Gd^{3+} spins to their $m_S = \pm 1/2$ sub-states, reducing the system to an 8-state subspace while retaining the essential physics of chiral spin textures.

The $S = 1/2$ doublets provide a platform for chiral qubit implementation via $\delta m_S = \pm 1$ transitions. Although high magnetic fields (e.g., Q-band EPR) improve spectral resolution, they require impractical electric potentials to overcome Zeeman dominance and induce finite scalar chirality (χ) via DM interactions. In contrast, X-band EPR regimes (~ 9.5 GHz, $B_0 \approx 0.34$ T) enable viable chirality control with moderate fields: the electric field breaks inversion symmetry to activate DM coupling, while the magnetic field lifts time-reversal degeneracy. The polarizable radical bridge makes the DM vector $\mathbf{D}_{ij}(E)$ highly sensitive to electric fields. At X-band frequencies, the reduced Zeeman energy ($E_Z = g\mu_B B_0$) allows DM interactions to dominate at lower E -field thresholds, governed by the

ratio $|\mathbf{D}_{ij}(E)/E_Z| \sim \lambda \cdot E \cdot r_{ij}/g\mu_B B_0 > 1$, where λ is the spin-electric coupling strength and r_{ij} is the interspin distance. A chiral qubit requires alternating chirality ($+\chi, -\chi$). Entangling two such qubits suppresses always-on interactions via phase interference ($\langle \psi | \sigma_z^A \sigma_z^B | \psi \rangle = 0$), while the chirality sequence must follow $+\chi, -\chi, -\chi, +\chi$ or $-\chi, +\chi, +\chi, -\chi$.

The energy spectrum and scalar chirality (χ), computed using Eq. 7, are shown in Fig. 5. The lowest doublets exhibit significant chirality ($\chi = \mp 0.18$, $\chi = \pm 0.13$), arising from DM-induced spin non-collinearity. Experimentally, the system can be initialized in the ground state, with selective excitations populating the projected basis. The four lowest-energy states (two chiral doublets) form a two-qubit system with quenched always-on interactions. Two distinct chiral-qubit transitions, resolvable at X-band frequencies (Fig. 5b), are energy-split due to time-reversal symmetry breaking and $\mathbf{D}(E)$ -dependent chirality. This enables entangled states, as demonstrated in our model.

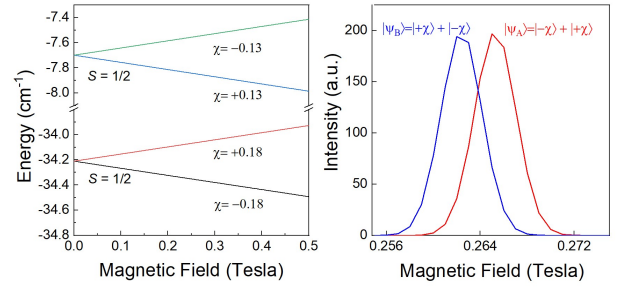


Figure 5: Left) Evolution of spin energy levels for two excited doublet forming chiral subspace. Right)- Two distinct chiral-qubit transitions, resolvable at X-band frequency of EPR.

3 Conclusion

We have developed a theoretical framework for engineering and controlling spin chirality in molecular quantum systems, leveraging the interplay of antiferromagnetic exchange, symmetry-breaking Dzyaloshinskii-Moriya (DM) interactions, and external magnetic fields. Our minimal three-spin model demonstrates that chiral ground states with nonzero scalar spin chirality ($\chi = \mathbf{S}_1 \cdot (\mathbf{S}_r \times \mathbf{S}_2)$) emerge as robust chiral qubits, intrinsically suppressing always-on interactions. Through Liouville–von Neumann dy-

namics, we revealed that these chiral qubits exhibit stable phase differences in superposition states. Applying our theoretical framework to realistic radical-bridged dinuclear lanthanide complexes, we demonstrates how spin-orbit coupling and asymmetric exchange permit electrical tuning of chirality, a step forward towards scalable molecular quantum technologies. These results establish chirality engineering as a versatile strategy to break inversion symmetry and time-reversal symmetry, which mitigates persistent interactions in multi-qubit systems, offering a pathway towards fault-tolerant quantum gates and networks. These results establish chirality engineering as a versatile strategy to mitigate persistent interactions in multi-qubit systems, offering a pathway toward fault-tolerant quantum gates and networks. Future work will explore chiral state manipulation via microwave pulses and strain, further bridging theory with experimental realizations.

4 Acknowledgements

A. G. A. has been supported by the Generalitat Valenciana (GVA) CIDEAGENT/2021/018 grant. The financial support by the Generalitat Valenciana (grant no. MFA/2022/017 and CIDEAGENT/2021/018) is gratefully acknowledged. Project MFA/2022/ 017 forms part of the Advanced Materials program supported by MICIU with funding from European Union NextGenerationEU (PRTR-C17.I1) and by Generalitat Valenciana.

References

- [1] See-Hun Yang, Ron Naaman, Yossi Paltiel, and Stuart SP Parkin. Chiral spintronics. *Nature Reviews Physics*, 3(5):328–343, 2021.
- [2] Clarice D Aiello, John M Abendroth, Muneer Abbas, Andrei Afanasev, Shivang Agarwal, Amartya S Banerjee, David N Beratan, Jason N Belling, Bertrand Berche, Antia Botana, et al. A chirality-based quantum leap. *ACS nano*, 16(4):4989–5035, 2022.
- [3] Jochen R Brandt, Francesco Salerno, and Matthew J Fuchter. The added value of small-molecule chirality in technological applications. *Nature Reviews Chemistry*, 1(6):0045, 2017.
- [4] Ron Naaman, Yossi Paltiel, and David H Waldeck. Chiral molecules and the electron spin. *Nature Reviews Chemistry*, 3(4):250–260, 2019.
- [5] Alessandro Chiesa, Alberto Privitera, Emilio Macaluso, Matteo Mannini, Robert Bittl, Ron Naaman, Michael R Wasielewski, Roberta Sessoli, and Stefano Carretta. Chirality-induced spin selectivity: An enabling technology for quantum applications. *Advanced Materials*, 35(28):2300472, 2023.
- [6] David Lujan, Jeongheon Choe, Swati Chaudhary, Gaihua Ye, Cynthia Nnokwe, Martin Rodriguez-Vega, Jiaming He, Frank Y Gao, T Nathan Nunley, Edoardo Baldini, et al. Spin-orbit exciton-induced phonon chirality in a quantum magnet. *Proceedings of the National Academy of Sciences*, 121(11):e2304360121, 2024.
- [7] Alessandro Chiesa, Mario Chizzini, E Gallati, E Salvadori, Francesco Tacchino, Paolo Santini, Ivano Tavernelli, Robert Bittl, M Chiesa, R Sessoli, et al. Assessing the nature of chiral-induced spin selectivity by magnetic resonance. *The Journal of Physical Chemistry Letters*, 12(27):6341–6347, 2021.
- [8] Alberto Privitera, Emilio Macaluso, Alessandro Chiesa, Alessio Gabbani, Davide Faccio, Demetra Giuri, Matteo Briganti, Niccolò Giaconi, Fabio Santanni, Nabila Jarmouni, et al. Direct detection of spin polarization in photoinduced charge transfer through a chiral bridge. *Chemical Science*, 13(41):12208–12218, 2022.
- [9] Mircea Trif, Filippo Troiani, Dimitrije Stepanenko, and Daniel Loss. Spin-electric coupling in molecular magnets. *Physical review letters*, 101(21):217201, 2008.
- [10] Mircea Trif, Filippo Troiani, Dimitrije Stepanenko, and Daniel Loss. Spin electric effects in molecular antiferromagnets. *Physical Review B*, 82(4):045429, 2010.
- [11] M Fhokrul Islam, Javier F Noss, Carlo M Canali, and Mark Pederson. First-principles study of spin-electric coupling in a {Cu 3} single molecular magnet. *Physical Review B*, 82(15):155446, 2010.
- [12] Florian Le Mardelé, Ivan Mohelský, Jan Wyzula, Milan Orlita, Philippe Turek, Filippo Troiani, and Athanassios K Boudalis. Probing spin-electric transitions in a molecu-

- p>lar exchange qubit.
- Nature Communications*
- , 16(1):1198, 2025.
- [13] Junjie Liu, Jakub Mrozek, Aman Ullah, Yan Duan, José J Baldoví, Eugenio Coronado, Alejandro Gaita-Ariño, and Arzhang Ardavan. Quantum coherent spin–electric control in a molecular nanomagnet at clock transitions. *Nature Physics*, 17(11):1205–1209, 2021.
 - [14] Clément Godfrin, Abdelkarim Ferhat, Rafik Ballou, Svetlana Klyatskaya, Mario Ruben, Wolfgang Wernsdorfer, and Franck Balestro. Operating quantum states in single magnetic molecules: implementation of grover’s quantum algorithm. *Physical review letters*, 119(18):187702, 2017.
 - [15] Bela E Bode, Edoardo Fusco, Rachel Nixon, Christian D Buch, Høgni Weihe, and Stergios Piligkos. Dipolar-coupled entangled molecular 4f qubits. *Journal of the American Chemical Society*, 145(5):2877–2883, 2023.
 - [16] Aman Ullah, Ziqi Hu, Jesús Cerdá, Juan Aragón, and Alejandro Gaita-Ariño. Electrical two-qubit gates within a pair of clock-qubit magnetic molecules. *npj Quantum Information*, 8(1):133, 2022.
 - [17] Grigore A Timco, Stefano Carretta, Filippo Troiani, Floriana Tuna, Robin J Pritchard, Christopher A Muryn, Eric JL McInnes, Alberto Ghirri, Andrea Candini, Paolo Santini, et al. Engineering the coupling between molecular spin qubits by coordination chemistry. *Nature Nanotechnology*, 4(3):173–178, 2009.
 - [18] Alejandro Gaita-Ariño, Fernando Luis, Stephen Hill, and Eugenio Coronado. Molecular spins for quantum computation. *Nature chemistry*, 11(4):301–309, 2019.
 - [19] Selvan Demir, Ie-Rang Jeon, Jeffrey R Long, and T David Harris. Radical ligand-containing single-molecule magnets. *Coordination Chemistry Reviews*, 289:149–176, 2015.
 - [20] Colin A Gould, K Randall McClain, Daniel Reta, Jon GC Kragoskow, David A Marchiori, Ella Lachman, Eun-Sang Choi, James G Ananlytis, R David Britt, Nicholas F Chilton, et al. Ultrahard magnetism from mixed-valence dilanthanide complexes with metal-metal bonding. *Science*, 375(6577):198–202, 2022.
 - [21] Ziqi Hu, Bo-Wei Dong, Zheng Liu, Jun-Jie Liu, Jie Su, Changcheng Yu, Jin Xiong, Di-Er Shi, Yuanyuan Wang, Bing-Wu Wang, et al. Endohedral metallofullerene as molecular high spin qubit: diverse rabi cycles in gd2@ c79n . *Journal of the American Chemical Society*, 140(3):1123–1130, 2018.
 - [22] Jeffrey D Rinehart, Ming Fang, William J Evans, and Jeffrey R Long. Strong exchange and magnetic blocking in n23 –radical-bridged lanthanide complexes. *Nature Chemistry*, 3(7):538–542, 2011.
 - [23] Ryogo Kubo. Stochastic liouville equations. *Journal of Mathematical Physics*, 4(2):174–183, 1963.
 - [24] Hongxin Yang, Jinghua Liang, and Qirui Cui. First-principles calculations for dzyaloshinskii–moriya interaction. *Nature Reviews Physics*, 5(1):43–61, 2023.
 - [25] Bo Luo, Juan Liu, and Kai-Lun Yao. Influences of dmi on spin-polarized current through a single-molecule magnet. *Physics Letters A*, 377(37):2428–2431, 2013.
 - [26] Veacheslav Vieru, Naoya Iwahara, Liviu Ungur, and Liviu F Chibotaru. Giant exchange interaction in mixed lanthanides. *Scientific Reports*, 6(1):24046, 2016.
 - [27] Daniel N Woodruff, Richard EP Winpenny, and Richard A Layfield. Lanthanide single-molecule magnets. *Chemical reviews*, 113(7):5110–5148, 2013.
 - [28] Jeffrey D Rinehart, Ming Fang, William J Evans, and Jeffrey R Long. A n23 –radical-bridged terbium complex exhibiting magnetic hysteresis at 14 k. *Journal of the American Chemical Society*, 133(36):14236–14239, 2011.
 - [29] Ignacio Fdez. Galvan, Morgane Vacher, Ali Alavi, Celestino Angeli, Francesco Aquilante, Jochen Autschbach, Jie J Bao, Sergey I Bokarev, Nikolay A Bogdanov, Rebecca K Carlson, et al. Openmolcas: From source code to insight. *J. Chem. Theory Comput.*, 15(11):5925–5964, 2019.
 - [30] Liviu Ungur and Liviu F Chibotaru. Ab initio crystal field for lanthanides. *Eur. J. Chem.*, 23(15):3708–3718, 2017.